

1 **Stability of the regional stress field in central Japan during the late Quaternary**

2 **inferred from the stress inversion of the active fault data**

3

4 **Hiroyuki Tsutsumi<sup>1</sup>, Katsushi Sato<sup>1</sup>, and Atsushi Yamaji<sup>1</sup>**

5 <sup>1</sup>Division of Earth and Planetary Science, Graduate School of Science, Kyoto University,

6 Kyoto 606-8502, Japan

## 7 **ABSTRACT**

8 We analyzed 169 geological fault-slip data from 37 active faults in central Japan to  
9 investigate the late Quaternary stress field stability. Modern stress states have been  
10 documented with unprecedented accuracy; however, their stability over time scales  
11 beyond instrumental observations is inadequately understood. Because the stress field  
12 has changed in the geological past, we compared present stress conditions in central  
13 Japan, determined from geophysical observations, with conditions determined by  
14 inverting the fault-slip data from active faults that exhibited cumulative displacement  
15 for the past  $\sim 10^5$  years. The maximum stress axis obtained from fault-slip data trends  
16 ESE–WNW. This state of stress accounts for 97% of the data and supports the fact that  
17 oblique faults with reverse and strike-slip senses are interlaced in the region. The  
18 optimal stress is similar to the present stress state, indicating that the stress field in  
19 central Japan has been uniform and stable over the past  $\sim 10^5$  years.

20

## 21 **1. Introduction**

22 The crustal stress field is one of the most important parameters required to  
23 understand tectonics, but the secular variation or stability of tectonic stress is not  
24 adequately understood for the time scales of  $10^3$ – $10^5$  years. The World Stress Map  
25 (WSM) Project was the first coordinated effort to map tectonic stress fields worldwide  
26 [Zoback, 1992], and the WSM database released in 2008 [Heidbach *et al.*, 2010]  
27 contains three times as much stress data as that of the 1992 database. Most of the data  
28 sets used to derive the stress fields in the project are geophysical data such as those  
29 derived from the focal-mechanism solutions of earthquakes and wellbore breakout. In  
30 contrast, geological data such as fault-slip data and volcanic-vent alignment accounted

31 for only ~10% of the total data [Zoback, 1992; Heidbach *et al.*, 2010]. The geophysical  
32 data reveal stress fields on the time scales of  $10^0$ – $10^2$  years, whereas the geological data  
33 reveal stress fields over longer periods, usually  $10^5$  years or longer. Active faults are the  
34 clues that will help in filling the gap between the time scales of geophysical and  
35 geological observations because their intermittent but steadily growing displacements  
36 over the last  $10^3$ – $10^5$  years are evident from, e.g., geomorphology, paleoseismic  
37 trenching, and seismic-reflection profiling. Central Japan is suitable for crustal  
38 stress-field analyses on different time scales because it contains one of the world's  
39 highest-quality geophysical [e.g., Mazzotti *et al.*, 2001; Townend and Zoback, 2006;  
40 Terakawa and Matsu'ura, 2010] and geological [e.g., *The Research Group for Active*  
41 *Faults of Japan*, 1991; Nakata and Imaizumi, 2002] data sets.

42 Permanent regional strain in central Japan has been accommodated mainly by active  
43 faults, which form a dense network in the region [*The Research Group for Active Faults*  
44 *of Japan*, 1991; Nakata and Imaizumi, 2002] (Figure 1). Since the 1995 Kobe  
45 earthquake, most of the long and fast-slipping faults in the region have been studied  
46 extensively through a national active-fault research program, which has produced one of  
47 the most comprehensive active-fault data sets in the world. Therefore, non-Andersonian  
48 faults have gradually become clear; reverse and strike-slip faults are interlaced in this  
49 region. In addition, a few of these types of faults have trends subparallel to each other  
50 while exhibiting different dip angles: the Hanaore and Biwako-seigan faults represent  
51 such a pair and are interpreted as an example of strain partitioning (Figure 1). Active  
52 faulting and its relation to the stress field in central Japan have been a topic of debate  
53 [Huzita, 1968; Okada and Ando, 1979], but the coexistence of faults with different  
54 senses of motion makes inference difficult without the inclusion of a special type of

55 stress-tensor inversion, as described below.

56 Stress-tensor inversion is used to determine stress conditions from the fault-slip data.  
57 Each datum comprises the attitude of a fault and the slip direction on the fault plane  
58 [e.g., *Angelier, 1979*] (Figure 2a). However, the slip directions are seldom determined  
59 along the segments of active faults. Instead, the directions are vaguely documented in  
60 the terms of slip senses. For example, the slip direction of a reverse fault has an  
61 uncertainty of 180° with respect to the rake direction; the dip occurs at the center of  
62 possible slip directions for the footwall block (Figure 2b). Similarly, the slip direction of  
63 a strike-slip fault has an uncertainty of 180°, but the possible slip direction is horizontal  
64 from the center of the slip. A few active faults in central Japan are described as oblique  
65 reverse faults with sinistral or dextral components. The slip directions of these faults  
66 have an uncertainty of 90° (Figure 2c). A fault-slip data set for active faults in central  
67 Japan includes such deficiencies. *Lisle et al.* [2001] developed a pioneering  
68 stress-inversion method to deal with sense-only data. Recently, *Sato* [2006] developed a  
69 special type of stress-inversion method to deal with mixed set of complete and  
70 sense-only fault-slip data.

71 In this study, we apply *Sato's* [2006] method to the active fault data to derive the  
72 regional stress field in central Japan. Although the slip inversion of a single active fault  
73 was conducted by *Blenkinsop* [2006] for the Chelungpu fault that ruptured during the  
74 1999 Chi-Chi earthquake in Taiwan, this is the first study to reveal a regional stress field  
75 based on the stress inversion analysis of a large set of the active fault data. We show that  
76 central Japan is under an ESE–WNW compressional stress field with a small stress ratio,  
77  $\Phi = (\sigma_2 - \sigma_3) / (\sigma_1 - \sigma_3)$ , and that the regional stress field has been uniform and stable  
78 over the past  $\sim 10^5$  years.

79

## 80 **2. Tectonic setting**

81 To the east of the Japanese islands, the Pacific plate is subducted westward beneath  
82 the North American and Philippine Sea plates (Figure 1). Along the Nankai trough, the  
83 Philippine Sea plate has been subducting northwestward since the Pliocene or  
84 mid-Pleistocene [e.g., *Seno and Maruyama, 1984; Yamaji, 2000*]. In the study area, i.e.,  
85 the eastern part of the southwest Japan arc, north-trending reverse faults and  
86 northwest-trending left-lateral and northeast-trending right-lateral strike-slip faults are  
87 densely distributed (Figure 1). The offsets of dated geomorphic features indicate slip  
88 rates in the order of  $10^{-1}$  to  $10^0$  mm/yr for such faults [*The Research Group for Active*  
89 *Faults of Japan, 1991*]. Central Japan has a long historical earthquake record that has  
90 been systematically collected for several centuries [*Usami, 2003; Ishibashi, 2004*]. The  
91 area has experienced one reverse-slip and four strike-slip earthquakes that ruptured the  
92 surface since the 1891 Nobi earthquake (Figure 1).

93 Geodetic and seismological data show that the Japan arc is subject to an  
94 approximate E–W compression. *Mazzotti et al. [2001]* calculated the permanent  
95 deformation field in central Japan by subtracting short-term elastic deformation related  
96 to the locking of the plate interface along the Nankai trough from GPS observations,  
97 and they obtained the residual-deformation field indicating ESE–WNW shortening.  
98 *Townend and Zoback [2006]* reported that the maximum horizontal stress is oriented  
99 approximately toward ENE–WSW in southwest Japan. *Terakawa and Matsu'ura [2010]*  
100 used the centroid-moment-tensor data to show that the tectonic stress of the Japan arc is  
101 basically an E–W compression with the direction of intermediate principal stress  
102 changing from N–S in northeast Japan to vertical in southwest Japan.

103

### 104 **3. Data**

105       After the 1995 Kobe earthquake, the Headquarters for Earthquake Research  
106 Promotion (HERP) of the Japanese government selected approximately 100 inland  
107 active faults and conducted extensive geological and paleoseismological studies to  
108 assess their seismic potential. We compiled the fault-slip data from 36 active faults  
109 selected by HERP in the Chubu and Kinki districts, to the west of the  
110 Itoigawa–Shizuoka tectonic line and east of the Nojima fault that ruptured during the  
111 1995 Kobe earthquake (Figure 1). To exclude local-stress perturbation due to the  
112 collision of the Izu Peninsula with the main island of Japan [e.g., *Mazzotti et al.*, 2001;  
113 *Townend and Zoback*, 2006] from our regional stress analysis, we analyzed the data for  
114 the faults to the west of the Itoigawa–Shizuoka tectonic line, which is part of the  
115 postulated plate boundary between the North American and Eurasian plates [*Nakamura*,  
116 1983]. We examined data from paleoseismic trench walls, natural outcrops, and seismic  
117 reflection profiles in published reports and maps. To determine the stress regime for a  
118 time scale of  $10^5$  years, we compiled the data on faults that clearly offset geomorphic  
119 surfaces or strata of late Quaternary age dated by tephrochronology or radiometric  
120 methods. Therefore, we catalogued reliable fault orientations and slip senses at 166 sites  
121 along 36 faults (Table S1 in the auxiliary material). In addition, we catalogued the data  
122 from three sites along the Fukozu fault, the source fault of the 1945 Mikawa earthquake  
123 that was not selected by HERP but for which extensive paleoseismic trenching was  
124 conducted [e.g., *Sone and Ueta*, 1993].

125       The fault-slip data set used in this study had a few deficiencies. Slickenlines were  
126 observed to determine the rakes of slip vectors at only 11 sites out of 169. We obtained

127 the “complete” data for 11 sites, and the remaining sites produced “sense-only” data,  
128 which have the rake uncertainties of  $90^\circ$  or  $180^\circ$  (Figures 2b and c). Figures 2d–f  
129 illustrate the tangent-lineation diagrams [*Twiss and Gefell, 1990*], improved by *Sato*  
130 [2006], that display the fault attitude and possible slip directions of the complete and  
131 sense-only data. A complete datum is denoted by an arrow plotted by a  
132 lower-hemisphere, equal-area projection; the pole of the fault plane is depicted in the  
133 stereogram by the position of the arrow, which itself indicates the slip direction of the  
134 footwall block (Figure 2d). The inward and outward directions of the arrow indicate the  
135 reverse and normal senses of shear, respectively. Strike-slip faults are represented by  
136 such arrows that are directed perpendicular to the radial directions in the plot. A  
137 sense-only datum is denoted by a semicircle or fan, which indicates the possible slip  
138 direction of the footwall block (Figures 2e and f). Figure 3 shows the fault-slip data  
139 from the active faults in the study area; we recorded a large variation of fault attitudes  
140 from 169 sites distributed along 37 faults.

141

#### 142 **4. Stress inversion**

143 The stress-inversion method proposed by *Sato* [2006] was employed to determine  
144 the stress conditions that explain the mixed set of the complete and sense-only data. The  
145 method can deal with both the complete and sense-only data by placing tighter and  
146 looser constraints on the conditions, respectively. The Wallace–Bott hypothesis is  
147 assumed, as is customary: the slip directions of faults are assumed to be parallel to the  
148 resolved shear stresses (theoretical slip directions) on the fault planes, which are  
149 calculated from the fault attitudes and stress conditions. The fitness of arbitrary stress  
150 conditions to a datum, i.e., how preferable is the assumption for a fault, is defined as a

151 decreasing function of the misfit angle  $d$  between the theoretical and observed slip  
152 directions (Figure 2g). The threshold in the function  $d_T$  is set to  $30^\circ$  in this study. For the  
153 sense-only data, the misfit angles are measured from the center of possible slip  
154 directions, and the degrees of fit are equal within the possible range (Figures 2h and i).  
155 According to *Sato* [2006], all the types of fitness functions are normalized as  
156 probability-density functions in the parameter space of deviatoric stress, which is  
157 represented schematically as the heights of fitness values in Figures 2g–i. The degrees  
158 of fit are added over the entire set of the complete and sense-only data to provide a total  
159 fitness of stress conditions. The optimal stress conditions are searched to maximize the  
160 total fitness. Although the complete data are uncommon in our database (Figure 3 and  
161 Table S1), the large variation of fault orientations and large number of data enable us to  
162 obtain a stress state with a relatively high precision.

163 Figure 4 shows the optimal stress for our data. A reverse-faulting stress-regime with  
164 an ESE–WNW-trending  $\sigma_1$ -axis was found to be capable of explaining almost all the  
165 data. The stress ratio,  $\Phi = (\sigma_2 - \sigma_3) / (\sigma_1 - \sigma_3)$ , was determined to be 0.09, which means  
166 that the magnitude of  $\sigma_2$  is approximately equal to that of  $\sigma_3$ . In addition, Figure 4  
167 illustrates the uncertainty of the solution by plotting principal stress axes that have  
168 fitness values greater than 90% of those of the optimal solution. Because of the small  $\Phi$   
169 value (axial compressional stress), the  $\sigma_3$ -axis has a greater uncertainty than that of the  
170  $\sigma_1$ -axis. We calculated theoretical slip directions for the faults by assuming optimal  
171 stress; white arrows in Figure 5 denote these directions.

172

## 173 **5. Discussion**

174 Despite the large variation of fault orientations (Figures 1 and 3), stress inversion  
175 revealed that almost all the active faults in the study area are consistent with a  
176 reverse-faulting stress regime with ESE–WNW-trending  $\sigma_1$ -axis (Figure 5). The  
177 theoretical slip directions of the faults calculated with this optimal stress were consistent  
178 with all the data except for five of them. Some of these exceptions have fault planes  
179 nearly perpendicular to the optimal  $\sigma_1$ -axis. Theoretical slip directions on such fault  
180 planes are unstable as is shown by the radial pattern around the  $\sigma_1$ -axis in Figure 5.  
181 Therefore, small perturbations in fault attitudes can explain the large misfits.

182 The optimal stress ratio of 0.09 indicates that  $\sigma_2$  and  $\sigma_3$  have similar values. Such a  
183 state of stress allows the coexistence of reverse and strike-slip faults, provided that they  
184 have different fault orientations. Their coexistence puzzled previous researchers who  
185 inferred the stress field from active faults in Japan because they assumed Andersonian  
186 faulting [*Huzita*, 1968; *Okada and Ando*, 1979]. Consequently, they neglected the  
187 coexistence of reverse and strike-slip faults or they had to infer spatially or temporarily  
188 complicated stress fields.

189 Although the ESE–WNW compression determined from active faults in this study is  
190 generally the same as that proposed by *Huzita* [1968], we demonstrated that a single  
191 state of stress explains the fault-slip data from all sites except five of them. This means  
192 that the stress field in central Japan has been uniform and that the active faults have  
193 slipped in the same directions over the past  $\sim 10^5$  years. From the coexistence of reverse  
194 and strike-slip faults, we predicted that non-Andersonian, oblique-slip faulting is  
195 common in this region although the rakes of slip vectors were observed for only 10 of  
196 37 faults.

197 The reactivation of the pre-existing planes of weakness gives rise to the

198 non-Andersonian faulting of planes with a wide variety of orientations. *Kano* [2002]  
199 suggested that a few active faults are present in such planes in the Mesozoic  
200 accretionary complex in the northern part of the study area. For example, the left-lateral  
201 Yanagase fault (Figure 1) reactivated a kink plane of a map-scale chevron fold.  
202 Similarly, the right-lateral Hanaore fault (Figure 1) lies along the axial surface of a fold  
203 structure [*Kano*, 2002]. *Ito* [2006] obtained the apatite fission track ages of ~20 Ma for  
204 dikes intruded along the Yanagase fault, which provides a minimum age constraint for  
205 the fault. *Murakami and Tagami* [2004] conducted the zircon fission-track analysis of  
206 pseudotachylyte sampled from the Nojima fault (Figure 1). They suggested that the  
207 Nojima fault was already initiated at ~56 Ma. The active Median Tectonic Line (Figure  
208 1) follows part of the boundary between the Ryoke and Sanbagawa terranes that were  
209 accreted in the Mesozoic [*Hashimoto*, 1991]. Therefore, a few active faults in central  
210 Japan reactivated the pre-existing faults under the present-day stress regime.

211 Slip on the active faults catalogued in this study reflects the average stress regime  
212 in the late Quaternary. The inverted stress state determined in this study is principally  
213 consistent with that obtained by geodetic and seismological data [*Mazzotti et al.*, 2001;  
214 *Townend and Zoback*, 2006; *Terakawa and Matsu'ura*, 2010], suggesting that the stress  
215 state in central Japan has been uniform and stable for the past  $\sim 10^5$  years.

216

## 217 **6. Conclusions**

218 A dense distribution and an extensive data set of active faults in central Japan has  
219 provided us with an exceptional opportunity to invert the regional stress field over a  
220 time scale of  $\sim 10^5$  years. We obtained an optimal state of stress, which is essentially the  
221 same as that obtained by seismological and geodetic data, indicating that the stress field

222 in the eastern part of southwest Japan has been stable over the past  $\sim 10^5$  years.  
223 Moreover, the inversion results provide a clear explanation for the coexistence of  
224 reverse and strike-slip faults in central Japan. Geological observations suggest that a  
225 few active faults in central Japan reactivated pre-existing faults under the present-day  
226 stress regime.

227

## 228 **Acknowledgments**

229 We thank Ritsuko Matsu'ura at the Association for the Development of Earthquake  
230 Prediction for access to the literature on the active faults used in this study and Shigeru  
231 Sueoka for his assistance in compiling the active fault database. We are grateful to  
232 Richard Lisle and Robert Yeats for constructive reviews.

233

## 234 **References**

- 235 Angelier, J. (1979), Determination of the mean principal directions of stresses for a  
236 given fault population, *Tectonophysics*, 56, T17-T26.
- 237 Blenkinsop, T. G. (2006), Kinematic and dynamic fault slip analyses: implications from  
238 the surface rupture of the 1999 Chi-Chi, Taiwan, earthquake, *J. Struct. Geol.*, 28,  
239 1040-1050.
- 240 Hashimoto, M. (Ed.) (1991), *Geology of Japan*, Terra Scientific Publishing Company,  
241 Tokyo.
- 242 Heidbach, O, M. Tingay, A. Barth, J. Reinecker, D. Kurfeß, and B. Müller (2010),  
243 Global crustal stress pattern based on the World Stress Map database release 2008,  
244 *Tectonophysics*, 428, 3-15.
- 245 Huzita, K. (1968), Rokko movements and its appearance: intersecting structural patterns

246 of southwest Japan and Quaternary crustal movements, *Quaternary Res.*, 7, 248-260.  
247 (in Japanese with English abstract)

248 Ishibashi, K. (2004), Status of historical seismology in Japan, *Ann. Geophys.*, 47,  
249 339-368.

250 Ito, H. (2006), Early Miocene igneous activity around northern part of the Yanagase  
251 fault and constraints on its fault activity from fission-track thermochronology, *J. Geol.*  
252 *Soc. Japan*, 112, 612-615. (in Japanese with English abstract)

253 Kano, K. (2002), Steeply-plunging, map-scale folds in the Mino-Tanba Belt, Southwest  
254 Japan: origin of the Yanagase Fault as viewed from the basement structures, *J. Geol.*  
255 *Soc. Japan*, 108, 591-605. (in Japanese with English abstract)

256 Kikuchi, M., and H. Kanamori (1996), Rupture process of the Kobe, Japan, earthquake  
257 of Jan. 17, 1995, determined from teleseismic body waves, *J. Phys. Earth*, 44,  
258 429-436.

259 Lisle, R., T. Orife, and L. Arlegui (2001), A stress inversion method requiring only slip  
260 sense, *J. Geophys. Res.*, 106, 2281-2289.

261 Mazzotti, S., P. Henry, and X. Le Pichon (2001), Transient and permanent deformation  
262 of central Japan estimated by GPS: 2. Strain partition and arc-arc collision, *Earth*  
263 *Planet. Sci. Lett.*, 184, 455-469.

264 Murakami, M., and T. Tagami (2004), Dating pseudotachylyte of the Nojima fault using  
265 the zircon fission-track method, *J. Geophys. Res.*, 31, L12604,  
266 doi:10.1029/2004GL020211.

267 Nakamura, K. (1983), Possible nascent trench along the eastern Japan Sea as the  
268 convergent boundary between Eurasian and North American plates, *Bull. Earthq. Res.*  
269 *Inst. Univ. Tokyo*, 58, 711-722. (in Japanese with English abstract)

270 Nakata, T., and T. Imaizumi (Eds.) (2002), *Digital Active Fault Map of Japan*,  
271 University of Tokyo Press, Tokyo. (in Japanese)

272 Okada, A., and M. Ando (1979), Active faults and earthquakes in Japan, *Kagaku*, 49,  
273 158-169. (in Japanese)

274 Sato, K. (2006), Incorporation of incomplete fault-slip data into stress tensor inversion,  
275 *Tectonophysics*, 421, 319-330.

276 Seno, T., and S. Maruyama (1984), Paleogeographic reconstruction and origin of the  
277 Philippine Sea, *Tectonophysics*, 102, 53-84.

278 Shiono, K. (1977), Focal mechanisms of major earthquakes in southwest Japan and  
279 their tectonic significance, *J. Phys. Earth*, 25, 1-26.

280 Sone, K., and K. Ueta (1993), Trenching study of the Fukozu fault at Tokoji, Aichi  
281 Prefecture in 1988, *Active Fault Res.*, 11, 43-46. (in Japanese)

282 Terakawa, T., and M. Matsu'ura (2010), The 3-D tectonic stress fields in and around  
283 Japan inverted from centroid moment tensor data of seismic events, *Tectonics*, 29,  
284 TC6008, doi: 10.1029/2009TC002626.

285 The Research Group for Active Faults of Japan (Ed.) (1991), *Active Faults in Japan:*  
286 *Sheet Maps and Inventories (revised edition)*, University of Tokyo Press, Tokyo. (in  
287 Japanese with English abstract)

288 Townend, J., and M. D. Zoback (2006), Stress, strain, and mountain building in central  
289 Japan, *J. Geophys. Res.*, 111, B03411, doi: 10.1029/2005JB003759.

290 Twiss, R. J., and M. J. Gefell (1990), Curved slickenfibers - a new brittle shear sense  
291 indicator with application to a sheared serpentinite, *J. Struct. Geol.*, 12, 471-481.

292 Usami, T. (2003), *Materials for Comprehensive List of Destructive Earthquakes in*  
293 *Japan (latest edition)*, University of Tokyo Press, Tokyo. (in Japanese)

294 Yamaji, A. (2000), The multiple inverse method applied to meso-scale faults in  
295 mid-Quaternary fore-arc sediments near the triple junction off central Japan, *J. Struct.*  
296 *Geol.*, 22, 429-440.

297 Zoback, M. L. (1992), First- and second-order patterns of stress in the lithosphere: the  
298 World Stress Map project, *J. Geophys. Res.*, 97, 10703-11728.

299

### 300 **Figure captions**

301 Figure 1. Tectonic setting and distribution of active faults in the Kinki and Chubu  
302 districts of central Japan. The active fault traces (red lines) are from *Nakata and*  
303 *Imaizumi* [2002], and black arrows denote major strike-slip faults. Blue crosses  
304 denote the locations of outcrops, trench sites, and seismic-reflection profiles from  
305 where the fault-slip data were collected. Focal-mechanism solutions for historical  
306 surface-rupturing earthquakes are also shown by *Shiono* [1977] and *Kikuchi and*  
307 *Kanamori* [1996]: 1891 Nobi, 1927 Kita-Tango, 1945 Mikawa, 1948 Fukui, and  
308 1995 Kobe earthquakes. Active faults mentioned in the text are Biwako-seigan  
309 fault: BF, Fukozu fault: FF, Hanaore fault: HF, Median Tectonic Line: MTL,  
310 Nojima fault: NF, and Yanagase fault: YF. Other abbreviations are  
311 Itoigawa–Shizuoka tectonic line: ISTL, Kyoto: Ky, Nagoya: Na, Osaka: O. Inset  
312 shows the plate-tectonic setting of Japanese islands. Eurasian plate: EU, Izu  
313 Peninsula: IP, North American plate: NA, Pacific plate: PA, Philippine Sea plate:  
314 PH. Thick arrows denote convergence directions between the Pacific and North  
315 American plates and between the Philippine Sea and Eurasian plates.

316

317 Figure 2. Types of fault-slip data and their constraints on stress condition. Figure (a)

318 shows a complete fault-slip datum comprising the attitude and slip direction of the  
319 fault. The direction is indicated by slickenlines on the fault plane. Figures (b) and  
320 (c) show the “sense-only” data obtained from faults on which slickenlines are not  
321 observed but whose sense of faulting is known from, for example, fault scarps and  
322 stream offsets. Either strike-slip sense or dip-slip sense of shear is known in (b),  
323 and both are known in (c). The possible slip directions of the footwalls are  
324 constrained within the range indicated by the semicircle and quadrant drawn on the  
325 fault plane. Figures (d–f) show the fault-slip data expressed in tangent-lineation  
326 diagrams [Twiss and Gefell, 1990] improved by Sato [2006]. Panels (d), (e), and (f)  
327 correspond to (a), (b), and (c), respectively. Figures (g–i) are graphs showing the  
328 fitness functions (bold lines) used in stress inversion, which can deal with all the  
329 types of the fault-slip data to determine the state of stress responsible for the  
330 observed fault movements. Figure (g) shows a fault with the complete data and the  
331 misfit angle  $d$  is between the theoretical and observed slip directions. Figures (h)  
332 and (i) show the case of a sense-only datum and  $d$  is defined as the angle formed  
333 by the theoretical slip direction and the central line of the semicircle or the fan.

334

335 Figure 3. Tangent-lineation diagram of the complete and sense-only fault-slip data  
336 obtained from the active faults in the study area. See Figure 2 for the explanations  
337 of the symbols.

338

339 Figure 4. Paired stereograms showing the range of stress conditions admissible for the  
340 fault-slip data in Figure 3. The stress ratios and principal orientations of the  
341 conditions are indicated by rainbow colors and lower-hemisphere, equal-area

342 projections. Stars denote the optimal orientations. The small circles are the  
343 principal axes of stresses with fitness greater than 90% of that of the optimal  
344 solution.

345

346 Figure 5. Optimal stress axes (open stars) and calculated theoretical slip directions  
347 (white arrows) plotted on a tangent-lineation diagram with a lower-hemisphere,  
348 equal-area projection. The fault-slip data are the same as that in Figure 3. The  
349 fault-slip data shown in red are inconsistent with the theoretical slip directions.  
350 Note that most of the data agree with the theoretical slip directions.

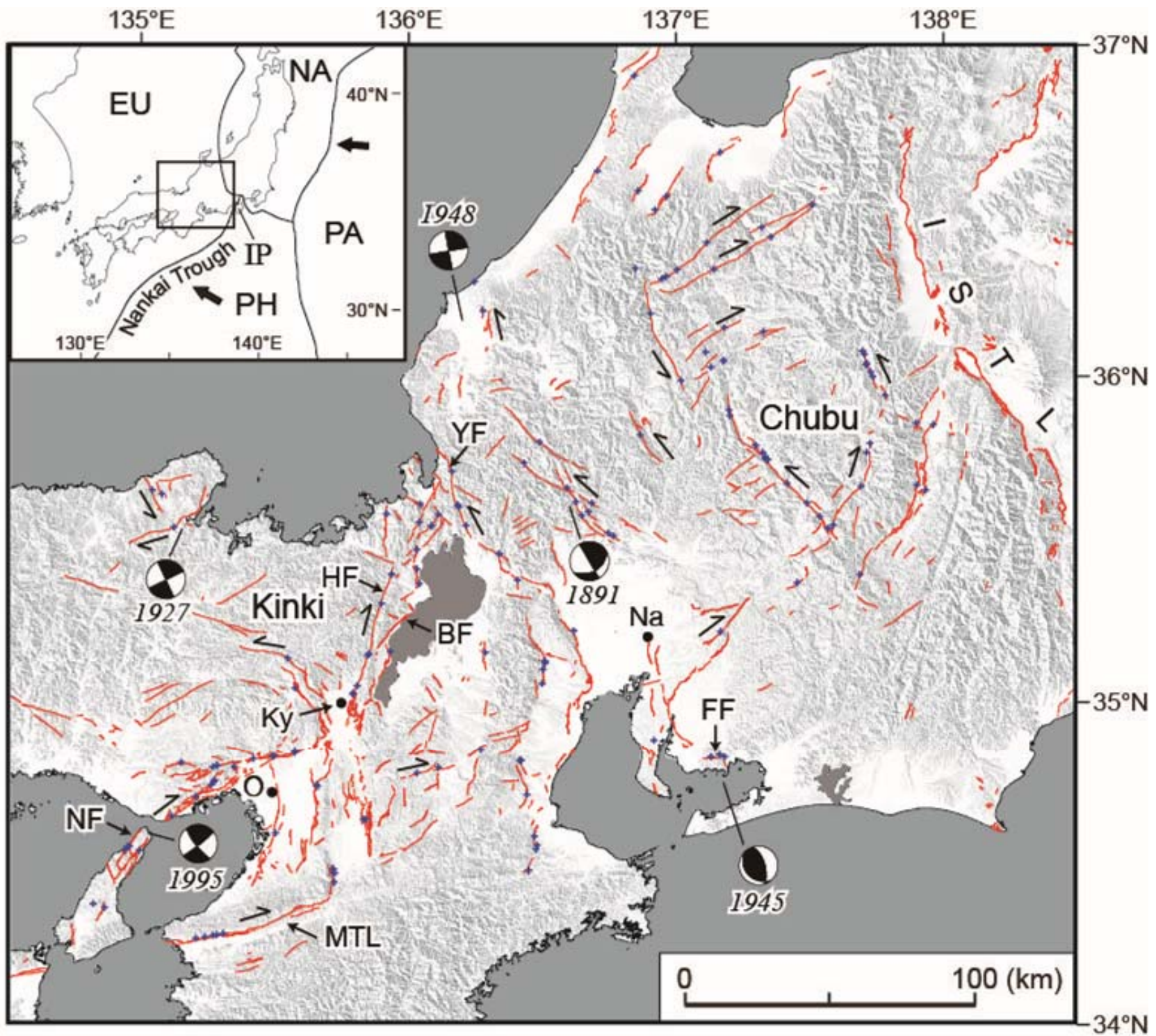


Figure 1.

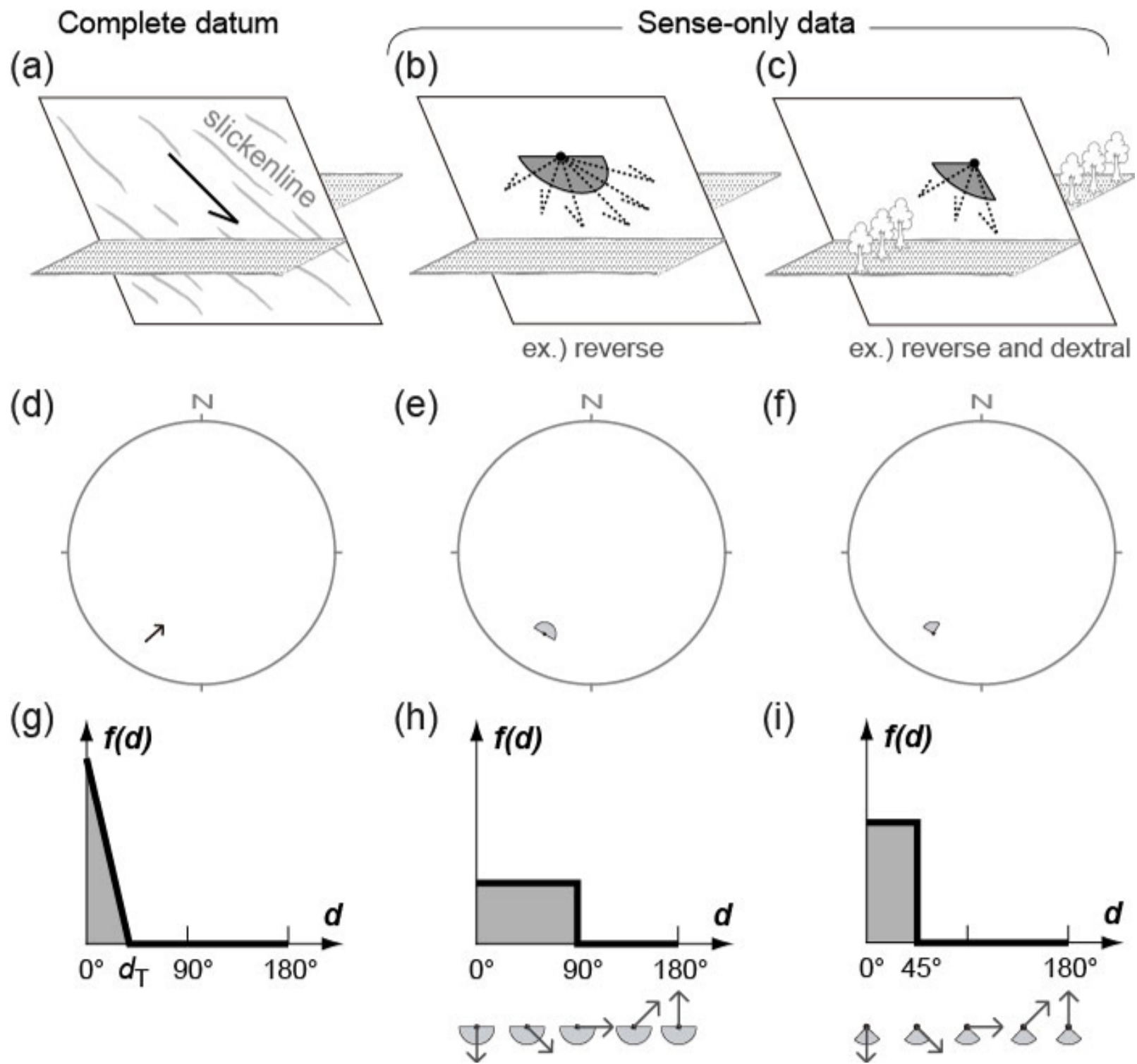


Figure 2.

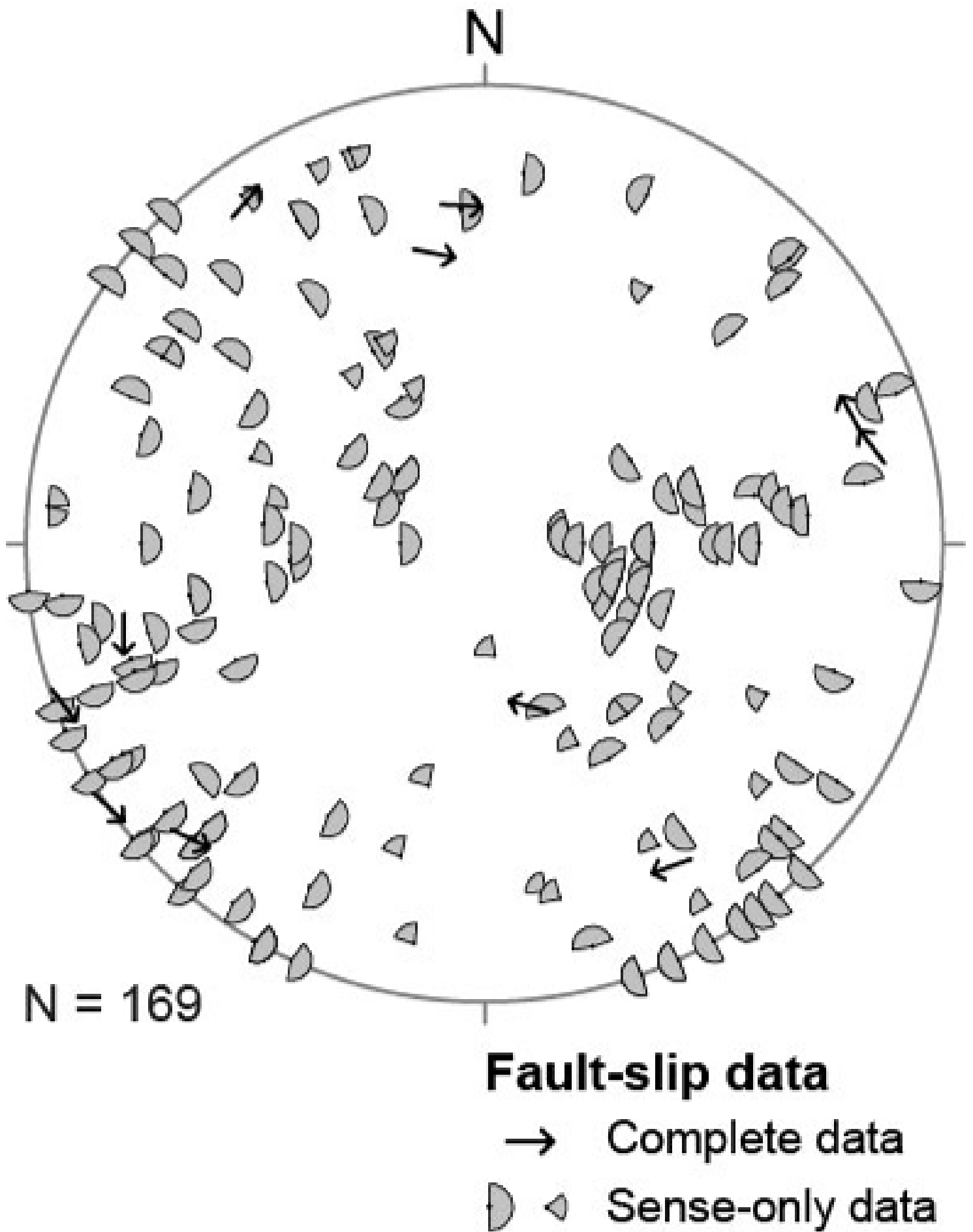


Figure 3.

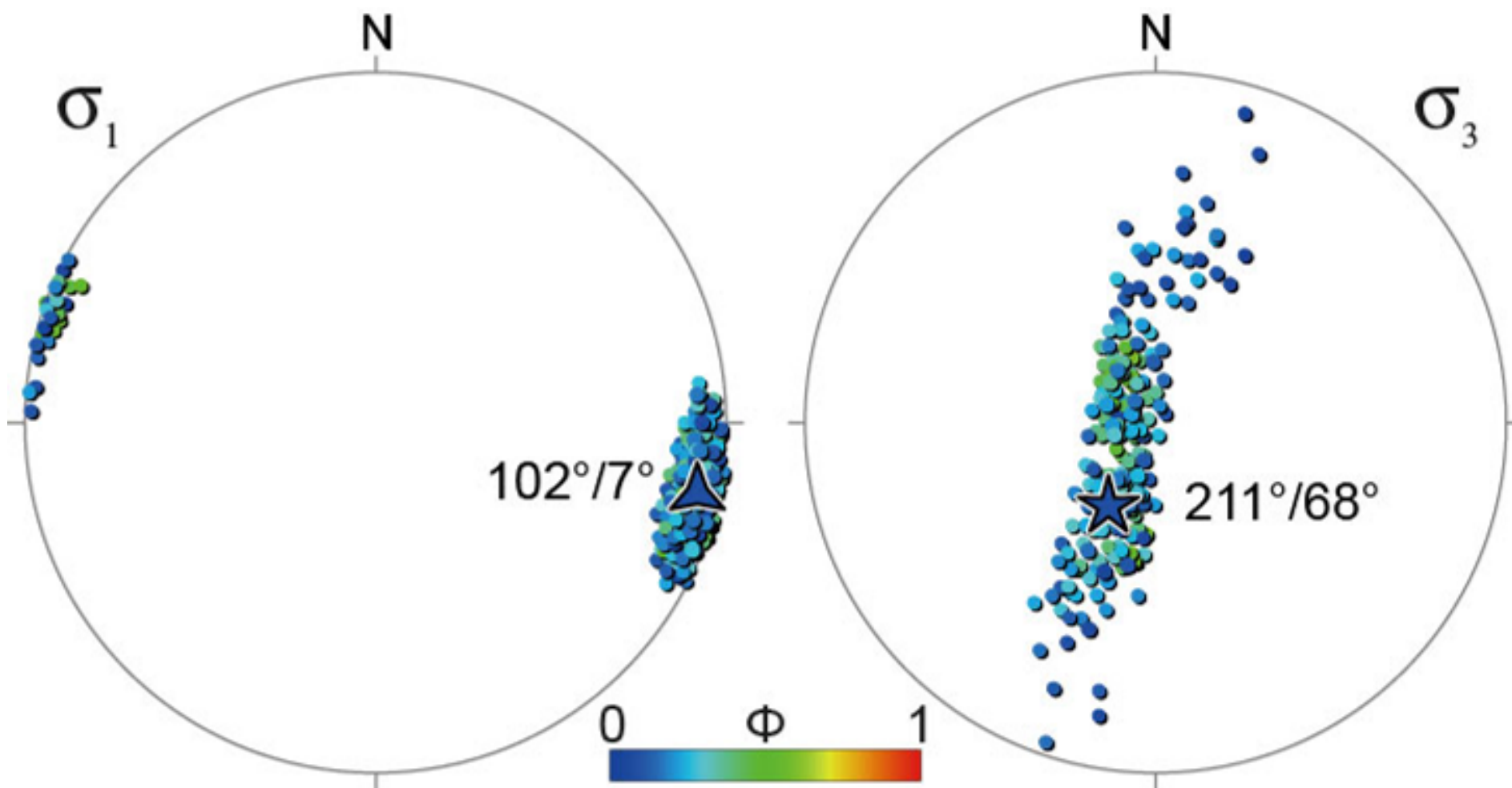
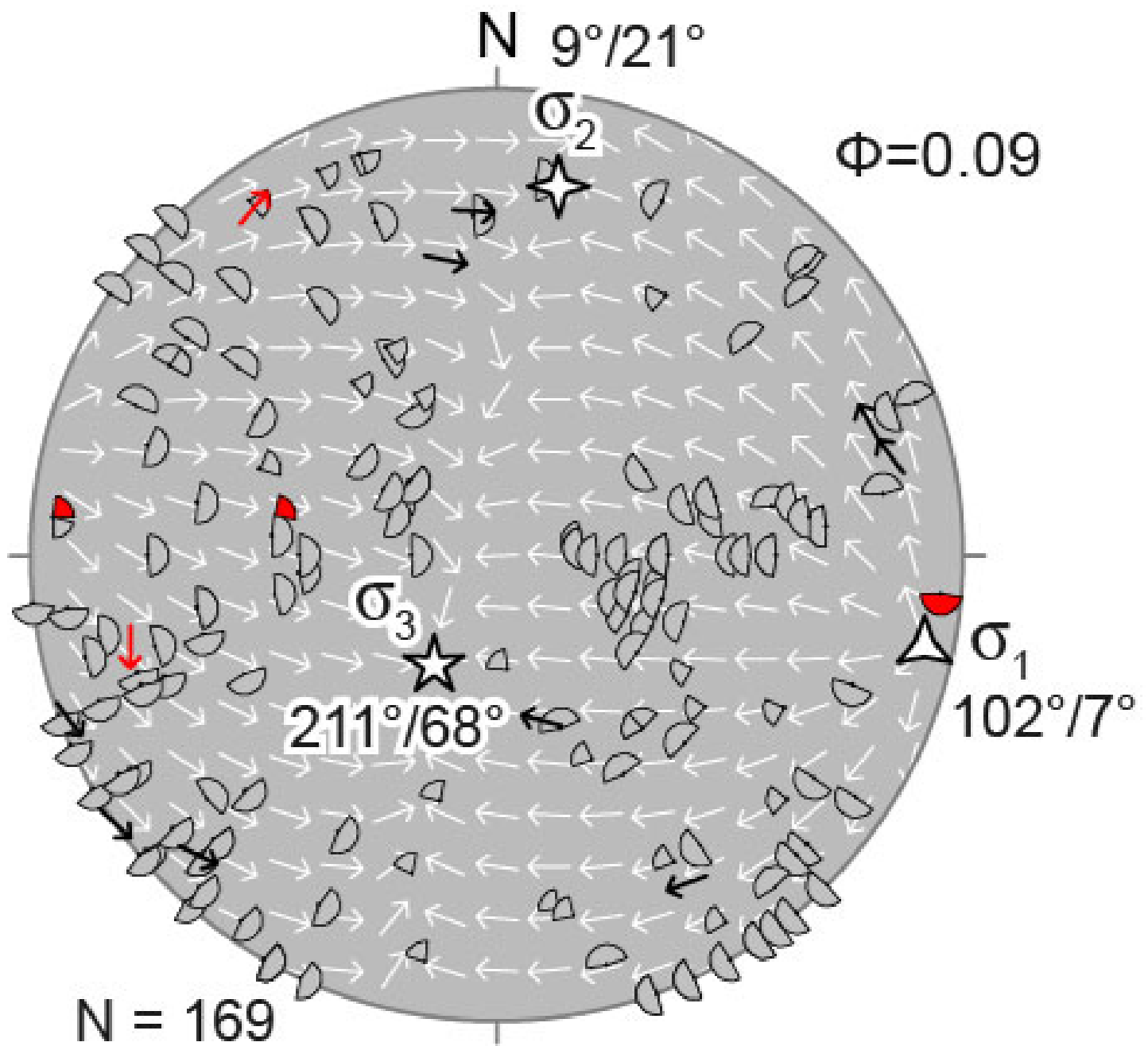


Figure 4.



**Fault-slip data**

with small misfit

with large misfit

Complete data



Sense-only data



→ Theoretical slip direction for optimal stress condition

Figure 5.

Table S1 Fault-slip data from 37 active faults in central Japan

Fault name (No. survey)	Name	Fault-slip data (Site No.)	Date source	Latitude (°N)	Longitude (°E)	Strike (°)	Sense of slip	Slip of slip vector)	Age of faulting(1)	Inversion analysis	Slip direction(2)	Slip orientation(3)						
										Weight	Remarks	Strike-slip	Normal	Reverse				
45	Etsumiyamaokami	45-1	natural outcrop	35.546	137.329	85E	right-lateral					175	0	0				
		45-2	natural outcrop	35.564	137.495	85E	right-lateral						144	55	0			
		45-3	tranching	35.705	137.247	85E	reverse, right-lateral						100	0	0			
		45-4	tranching	35.728	137.714	82E	reverse, right-lateral						115	29	0			
46	Saitama-Kanto	46-1	tranching	35.947	137.713	N20E	left-lateral						79	0	0			
		46-2	natural outcrop	35.802	137.781	N20E	left-lateral						238	0	0			
		46-3	tranching	35.835	137.769	N20E	left-lateral						70	0	0			
		46-4	natural outcrop	35.986	137.748	N20E	left-lateral						61	0	0			
		46-5	natural outcrop	35.879	137.668	N20E	left-lateral						0.5	close to 46-2	72	0	0	
		46-6	natural outcrop	35.873	137.693	N20E	left-lateral						0.5	close to 46-5	38	14	0	
		46-7	natural outcrop	35.838	137.715	N20E	left-lateral						1	76	79	353.1	18.7	
47	Atsugawa	47-1	tranching	36.325	137.137	N60E	right-lateral						138	79	245.2	34.1		
		47-2	natural outcrop	36.328	137.584	N20E	right-lateral						145	80	236.4	24.6		
		47-3	natural outcrop	36.453	137.543	N20E	right-lateral						137	0	0	0		
		47-4	natural outcrop	36.426	137.511	N20E	right-lateral						133	0	0	0		
48	Tateyama-Ogino	48-1	tranching	36.479	137.520	N60E	right-lateral						137	76	0	0		
		48-2	tranching	36.137	137.341	N70E	right-lateral						138	0	0	0		
		48-3	tranching	36.046	137.126	N70E	right-lateral						0.5	close to 48-4	315	80	0	
		48-4	tranching	36.043	137.121	N70E	right-lateral						0.5	close to 48-3	312	80	0	
		48-5	tranching	36.078	137.127	N70E	right-lateral						1	128	96	0	0	
49	Ishikubi	49-1	natural outcrop	36.291	136.943	N60E	right-lateral						138	79	0	0		
		49-2	natural outcrop	36.361	136.913	N60E	right-lateral						139	48	0	0		
		49-3	tranching	36.361	136.922	N60E	right-lateral						0.5	close to 49-2	315	80	0	
		49-4	tranching	36.369	136.936	N60E	right-lateral						0.5	close to 49-3	312	80	0	
50	Shikawa	50-1	natural outcrop	36.328	136.829	N30E	right-lateral						137	0	0	0		
		50-2	tranching	36.389	136.869	N30E	right-lateral						1	208	50	0	0	
		50-3	tranching	35.987	137.816	N20E	right-lateral						1	79	79	0	0	
		50-4	tranching	35.987	137.816	N20E	right-lateral						1	208	50	0	0	
51	Inabiri	51-1	satellite profiling	35.858	137.858	N30E	reverse						1	235	25	0		
		51-2	satellite profiling	35.821	137.812	N30E	reverse						1	235	25	0		
		51-3	tranching	35.821	137.812	N30E	reverse						1	235	25	0		
		51-4	tranching	35.821	137.812	N30E	reverse						1	235	25	0		
		51-5	tranching	35.821	137.812	N30E	reverse						1	235	25	0		
52	Awa	52-1	natural outcrop	35.897	137.185	N30E	right-lateral						84	96	0	0		
		52-2	natural outcrop	35.885	137.189	N30E	right-lateral						0.5	close to 52-1	89	88	137.0	29.5
		52-3	natural outcrop	35.743	137.207	N30E	right-lateral						1	77	72	0	0	
		52-4	tranching	35.787	137.292	N30E	right-lateral						0.5	close to 52-5	85	88	0	0
		52-5	tranching	35.782	137.282	N30E	right-lateral						0.5	close to 52-4	83	87	0	0
		52-6	natural outcrop	35.787	137.227	N30E	right-lateral						1	83	82	0	0	
		52-7	natural outcrop	35.793	137.218	N30E	right-lateral						1	83	82	0	0	
		52-8	tranching	35.745	137.246	N30E	right-lateral						1	85	75	0	0	
		52-9	tranching	35.827	137.217	N30E	right-lateral						1	85	75	0	0	
		52-10	natural outcrop	35.825	137.217	N30E	right-lateral						1	85	75	0	0	
		52-11	tranching	35.535	137.447	N30E	right-lateral						0.5	close to 52-12	228	80	0	0
		52-12	tranching	35.535	137.447	N30E	right-lateral						0.5	close to 52-11	228	80	0	0
53	Nishiyama-Ogino	53-1	tranching	35.369	137.424	N30E	right-lateral						148	48	0	0		
		53-2	tranching, borehole survey	35.273	137.433	N30E	right-lateral						1	148	48	0	0	
54	Sogayama	54-1	tranching, borehole survey	34.835	136.941	N30E	reverse						1	238	80	0		
		54-2	satellite profiling	34.835	136.941	N30E	reverse						1	238	80	0		
55	Dokugata	55-1	satellite profiling	36.026	136.867	N30E	reverse						0.5	close to 55-2	138	80	0	
		55-2	tranching	36.026	136.867	N30E	reverse						1	138	80	0		
		55-3	tranching	36.026	136.867	N30E	reverse						1	138	80	0		
56	Tomihata-Akashi	56-1	satellite profiling	36.363	136.854	N30E	reverse						1	115	47.5	0		
		56-2	tranching	36.249	136.888	N30E	reverse						1	118	28	0		
		56-3	tranching	36.265	136.883	N30E	reverse						1	118	28	0		
		56-4	tranching	36.265	136.883	N30E	reverse						1	118	28	0		
57	Nishiyama-Ogino	57-1	tranching	36.629	136.789	N30E	reverse						1	138	23	0		
		57-2	natural outcrop	36.281	136.237	N30E	reverse						1	78.5	76	0		
58	Fukuhirayama	58-1	natural outcrop	36.281	136.237	N30E	reverse						1	78.5	76	0		
		58-2	tranching	36.281	136.237	N30E	reverse						1	78.5	76	0		
59	Haganaga-Joryu	59-1	natural outcrop	35.822	136.929	N30E	right-lateral						1	85	72.5	0		
		59-2	tranching	35.822	136.929	N30E	right-lateral						1	85	72.5	0		
		59-3	tranching	35.822	136.929	N30E	right-lateral						1	85	72.5	0		
		59-4	tranching	35.822	136.929	N30E	right-lateral						1	85	72.5	0		
		59-5	tranching	35.822	136.929	N30E	right-lateral						1	85	72.5	0		
		59-6	tranching	35.822	136.929	N30E	right-lateral						1	85	72.5	0		
		59-7	tranching	35.822	136.929	N30E	right-lateral						1	85	72.5	0		
		59-8	tranching	35.822	136.929	N30E	right-lateral						1	85	72.5	0		
		59-9	tranching	35.822	136.929	N30E	right-lateral						1	85	72.5	0		
		59-10	tranching	35.822	136.929	N30E	right-lateral						1	85	72.5	0		
		59-11	tranching	35.822	136.929	N30E	right-lateral						1	85	72.5	0		
		59-12	tranching	35.822	136.929	N30E	right-lateral						1	85	72.5	0		
60	Nobi	60-1	tranching	35.822	136.929	N30E	right-lateral						1	85	72.5	0		
		60-2	tranching	35.822	136.929	N30E	right-lateral						1	85	72.5	0		
		60-3	tranching	35.822	136.929	N30E	right-lateral						1	85	72.5	0		
		60-4	natural outcrop	35.822	136.929	N30E	right-lateral						1	85	72.5	0		
		60-5	tranching	35.822	136.929	N30E	right-lateral						1	85	72.5	0		
		60-6	tranching	35.822	136.929	N30E	right-lateral						1	85	72.5	0		
		60-7	tranching	35.822	136.929	N30E	right-lateral						1	85	72.5	0		
		60-8	tranching	35.822	136.929	N30E	right-lateral						1	85	72.5	0		
		60-9	tranching	35.822	136.929	N30E	right-lateral						1	85	72.5	0		
		60-10	tranching	35.822	136.929	N30E	right-lateral						1	85	72.5	0		
		60-11	natural outcrop	35.822	136.929	N30E	right-lateral						1	85	72.5	0		
		60-12	natural outcrop	35.822	136.929	N30E	right-lateral						1	85	72.5	0		
61	Tomihata-Akashi	61-1	natural outcrop	35.822	136.929	N30E	right-lateral						1	85	72.5	0		
		61-2	natural outcrop	35.822	136.929	N30E	right-lateral						1	85	72.5	0		
		61-3	natural outcrop	35.822	136.929	N30E	right-lateral						1	85	72.5	0		
		61-4	natural outcrop	35.822	136.929	N30E	right-lateral						1	85	72.5	0		
62	Saitama-Kanto	62-1	natural outcrop	35.947	137.713	N20E	left-lateral						79	0	0			
		62-2	natural outcrop	35.802	137.781	N20E	left-lateral						238	0	0			
		62-3	tranching	35.835	137.769	N20E	left-lateral						70	0	0			